Structural, optical and mechanical properties of AlN films - effect of thickness

M. Jergel[D], C. Falcony
Departamento de Física, CINVESTAV-IPN, Apdo Postal 14-740, 07300 México, D.F., México

M. Aguilar-Frutis
CICATA-IPN, Miguel Hidalgo, 11500 México, D.F., México

M.A. Auger, O. Sanchez, J.M. Albella
Instituto de Ciencia de Materiales de Madrid (CSIC), 28049 Cantoblanco, Madrid, Spain

Highly stoichiometric hexagonal AlN films of different thicknesses ranging from ≈10 nm to >1 μm were synthetized on silicon (100) substrates under the same deposition conditions by dc reactive magnetron sputtering. The X-ray diffraction and reflectometry, ellipsometry, scanning electron and atomic force microscopies, and nanoindentation techniques were applied to study the effect of the film thickness on the structure, refractive index and hardness. Fine granular structure transforms into the ordered columnar form possessing (002) texture with increasing film thickness, the refractive index being affected only slightly. The most notable feature is the existence of a particular film thickness around 800 nm where the texture perfection reaches a maximum. This result was verified on a repeatedly deposited film of the same thickness. The texture extreme at 800 nm brings about a significant hardness enhancement which surpasses 20 GPa, presumably due to the hampered dislocation formation and/or motion.

Keywords: AlN thin film; X-ray diffraction; ellipsometry; Nanoindentation; Columnar texture; Hardness
PACS: 61.10.Eq; 62.20.Qp; 68.55.Jk; 81.15.Cd

1. Introduction

AlN thin films are used in a wide variety of applications such as electroacustic and optical devices, thermal conductors, protective coatings, and insulating layers [1-3]. It was found that preferrential orientation of polycrystalline AlN films affects and often improves the properties of practical use such as piezoelectricity [4] or hardness [5]. A low surface roughness is also required. Hence, it is important to study the conditions under which highly oriented AlN thin film structures with a low surface roughness can be grown. Different techniques have been used to deposit AlN films, amongst them chemical vapour deposition, molecular beam epitaxy, pulsed laser deposition or reactive magnetron sputtering [6-8]. The substrate type and deposition conditions have proved to be important for the growth of well aligned grains. In this paper, we investigate the effect of the film thickness on the structure and surface morphology on a series of AlN films prepared under the same conditions on the same type of the substrate. The study is completed by hardness and ellipsometry measurements.

2. Experimental

The deposition was performed onto silicon (100) substrate at room temperature in a balanced dc magnetron sputtering system. Reactive sputtering was produced on a high-purity (99.999%) aluminium target, operated at 100W DC cathode power and 6,5cm away from the substrate. The vacuum pumping system consisted of a turbomolecular pump backed by a mechanical pump which provided a base pressure lower than 10^{-6}mbar; the working pressure was 2-$4x10^{-3}$mbar. Argon and nitrogen gases were introduced into the chamber by separated mass flow controllers. The deposition conditions providing 1:1 stoichiometry were reached after correlating the nitrogen incorporation in the layer to the argon/nitrogen ratio in the sputtering gas, as described in our previous study [9]. The different argon/nitrogen ratios studied ranged from 96%/4% to 15%/85%, and the RBS and ERDA results showed that the ratio 20%/80% (5.9sccm/23.6sccm) provided AlN_x films with x~1 at ~50Å/min deposition rate. These flow rate conditions were used for all samples, which were grown at different deposition times to get the different layer thicknesses studied in the present work. The final film thickness was checked by a Dektak 3030 profilometer (Table 1) and these values are taken below as the nominal thicknesses to identify the samples.

The atomic structure inside the layers was examined by X-ray diffraction (XRD). The XRD measurements at CuK_α wavelength were performed on Siemens D 5000 diffractometer both in Bragg-Brentano (BB) and surface-sensitive grazing incidence (GI) modes. The angle of incidence in GI mode was set to 0.5°, 1°, 1.5°. This angle controls the sample depth which primarily contributes to the diffracted intensity. The microstructure and surface morphology of the layers were inspected by scanning electron microscopy (SEM) and atomic force microscopy (AFM), respectively. The X-ray reflectivity (XRR) measured on a high-resolution Stoe diffractometer at

---

[D] on the leave from the Institute of Physics, Slovak Academy of Sciences, Bratislava, Slovakia

Table 1. Thicknesses of the films determined by the Dektak profilometry, ellipsometry, and X-ray reflectivity. The refractive index measured by ellipsometry is indicated in the last column.

Sample	**Thickness** (nm)			Refractive Index
	Profilometry	Ellipsometry	XRR	
AlN31	≈ 10	16.3 ± 1.4	15.8 ± 0.1	1.883 ± 0.133
AlN33	46	59.7 ± 0.2	60.0 ± 0.1	1.993 ± 0.003
AlN27	150	135.8 ± 11.2	176.0 ± 0.2	---
AlN36	200	245.2 ± 3.1	256. 0± 0.2	1.871 ± 0.025
AlN34	600	627.5 ± 7.8	---	1.861 ± 0.018
AlN16	800	793.8 ± 69	---	1.871 ± 0.072
AlN35	1585	1508.4 ± 5.3	---	1.902 ± 0.008

$CuK_{\alpha 1}$ wavelength provided an additional information on the surface roughness and the film thickness. The latter parameter, together with the refractive index, was obtained also from ellipsometry measurements performed on Gaertner L117 ellipsometer at 632.8 nm wavelength and at an incidence angle of 70º. Finally, the film hardness was determined in a Nanotest Berkovitch indenter with variable load ranges in order to get an indentation depth profile.

3. Results

The polycrystalline hexagonal structure of wurtzite type (file No. 25-1133 of JCPDS-ICDD diffraction database PDF-2) was detected in the films by XRD. An example of GI diffraction pattern for the film 200 nm thick is shown in Fig. 1. Here the diffractions coming from the film monotonically decrease while that one of the substrate increases with increasing angle of incidence α. With increasing film thickness, an optimum balance between the absorption path and the irradiated volume of the film is shifted to larger incidence angles. Consequently, the film diffractions reach maximum intensity level at the incidence angles α>0.5°. Only one broad peak around the position of 002 diffraction was detected at a very grazing angle of incidence α=0.3° for the thinnest film of ≈10 nm thickness which suggests the presence of a fine granular structure. The diffraction patterns of this sample could not be evaluated numerically.

As it can be seen from Fig. 1, the relative diffraction intensities are markedly different from those of the random polycrystalline bulk phase, some diffractions being even absent, which is the case also of other samples. The 002 diffraction is always the strongest one both in GI and BB diffraction patterns (Fig. 2) which may be understood in view of a broad rocking curve, measured with the detector fixed at the position of 002 diffraction, which stretches up to the grazing incidence/exit regions (Fig.3). These facts indicate a preferred orientation of (001) planes parallel to the substrate. Such one axial hexagonal texture with c axis perpendicular to the substrate has been detected in AlN films previously [10-12] and usually is connected with the columnar film growth which we observed by SEM (Fig. 4).

Table 2. Ratio of the integral intensities of the 001 and 101 diffractions in the BB diffraction patterns.

sample	AlN36	AlN34	AlN16	AlN35
I_{002}/I_{101}	5.5	40.0	∝	4.7

The texture perfection can be quantified by the full width at half maximum (FWHM) value of the rocking curve measured on the characteristic texture diffraction. In our case, a texture comparison between different films based on this FWHM value was precluded by different rocking curve shapes. While the rocking curves of the films 600 nm thick and more have a typical bell-like shape, those of the thinner films are composed of a central ridge superimposed on a broad background (Fig. 3). Obviously, a sharper rocking curve and a much broader one are present together, the former and the latter coming presumably from well oriented grains inside the columns and more random matrix outside, respectively. Therefore we compared the texture perfection from the ratio of the integral intensities of the 002 and 101 diffractions (Table 2), in fact the strongest ones in BB diffraction patterns. As the (101) planes make a large angle with the (001) ones (61.58° in the hexagonal lattice of bulk AlN), the 101 diffraction is competitive to the 002 one in terms of texture and the ratio is thus directly related to the contribution of the hexagonal (002) texture component. Still more competitive 100 and 110 diffractions (from the planes making 90° angle with the (001) one) were too weak to be used. The ratio could not be evaluated in the films 46 nm and 150 nm thick where the 101 diffraction is hidden in the background.

The *a* and *c* lattice parameters of the films determined from the XRD are larger and smaller, respectively, in comparison with the unstrained bulk phase (Table 3). In the presence of one axial texture along c axis perpendicular to the substrate, such a macrostrain leads to a tensile in-plane stress in the film. The lattice distortion is at maximum in

Table 3. Comparison of the lattice parameters with those of the unstrained bulk phase calculated as $\Delta = (a_{film} - a_{bulk})/ a_{bulk}$. The reference lattice parameters of the bulk phase are indicated in the last line.

sample	Δa (%)	Δc (%)
AlN33	+ 0.85	- 0.64
AlN27	+ 0.53	- 0.32
AlN36	+ 0.51	- 0.33
AlN34	+ 0.38	- 0.24
AlN16	+ 0.39	- 0.22
AlN35	+ 0.38	- 0.21
bulk	0.31114 nm	0.49792 nm

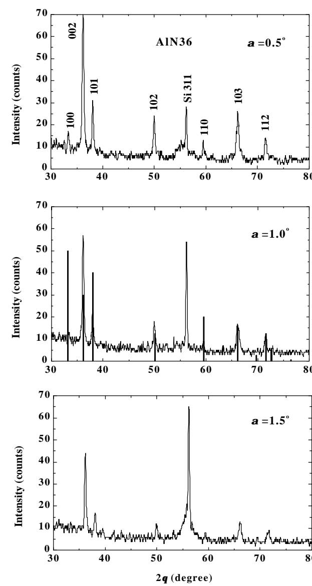

Figure 1. Grazing incidence diffraction patterns of the film 200 nm thick at different angles of incidence ***a***. The bars in the middle pattern show the positions and relative intensities of the diffractions for hexagonal AlN phase according to the JCPDS-ICDD diffraction database PDF-2.

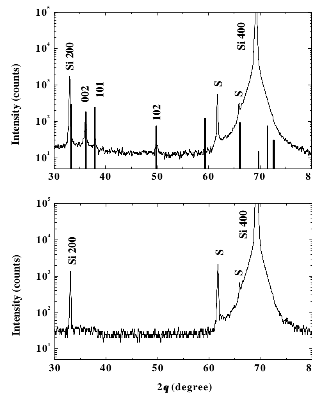

Figure 2. Bragg-Brentano diffraction pattern of the film 200 nm thick. The bars have the same meaning as in Fig. 1. In addition to regular Si 400 diffraction coming from the substrate, "forbidden" Si 200 one is detected. The unidentified diffractions labelled as "S" come also from the substrate as the lower pattern measured on the bare substrate proves. Note that differently to Fig. 1, the intensity scale is logarithmic.

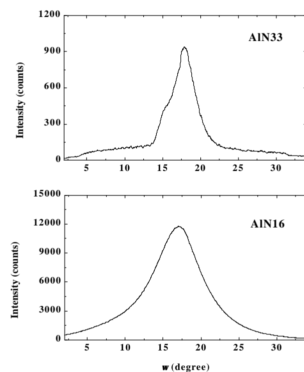

Figure 3. Rocking curves of the films 46 nm and 800 nm thick measured with the detector fixed at the 002 diffraction angle. The angle ***w*** is the incidence angle measured from the sample surface.

Table 4. Grain size *D* and rms value of microstrain $\sqrt{\langle e^2 \rangle}$ determined from the Williamson-Hall plot.

Sample	*D* (nm)	$\sqrt{\langle e^2 \rangle}$
AlN33	30.4 ± 3.5	$(4.15 \pm 0.65)\times10^{-3}$
AlN27	41.9± 3.5	$(2.33 \pm 0.39)\times10^{-3}$
AlN36	42.3 ± 1.7	$(2.71 \pm 0.18)\times10^{-3}$
AlN34	39.6 ± 0.6	$(2.64 \pm 0.07)\times10^{-3}$
AlN16	85.5 ± 19	$(3.09 \pm 0.45)\times10^{-3}$
AlN35	43.6 ± 2.3	$(2.41 \pm 0.23)\times10^{-3}$

the 46 nm thick film and gradually is relieved with increasing film thickness.

The Williamson-Hall plot (Fig. 5) [13] enables us to determine the grain size and microstrain, which both contribute to the diffraction line broadening, in a rather simple way. The results of this analysis are gathered in Table 4. There is no systematic thickness dependence of the grain size which oscillates around 40 nm, however, the grain size in the film 800 nm thick is approximately twice of that in other films. On the other hand, the value for the film 46 nm thick is ≈10 nm below the average. Though it could not be evaluated, the grain size in the ≈10 nm thick film without distinct diffraction peaks is obviously still smaller and limited by the film thickness. The root-mean-square (rms) value of microstrain in the 46 nm thick film is apparently larger than in the thicker films, otherwise there is no systematic dependence on the film thickness.

The surface roughness of the films evaluated from AFM measurements (Table 5) shows a monotonic increase with increasing thickness. The two thinnest films exhibit extremely low values, probably due to the small grains. On the other hand, the 800 nm thick film has nearly the same roughness as the thickest one due to the largest grains. A difference between the surface morphologies of the thin and thick films can be seen in Fig. 6.

For thinner films, the surface roughness could be evaluated also from the simulations of the XRR curves and the values are in a reasonable agreement with AFM results (Table 5). The film thicknesses determined from the XRR simulations are shown in Table 1. For thicker films, the XRR oscillations were too dense to arrive at reliable simulations.

The refractive index as well as the thicknesses of the films were determined by ellipsometry (Table 1). At the wavelength used, the films are transparent (AlN is non-absorbing in the ***l***>550nm spectral region). For thinner films, the thickness values obtained by the ellipsometry (and also by the XRR) are generally larger than those resulting from the Dektak profilometry (Table 1). This observation may be attributed to the fact that non destructive optical methods are sensitive also to the inner thin film/substrate interface whose width starts to play a role for small film thicknesses. On the other hand,

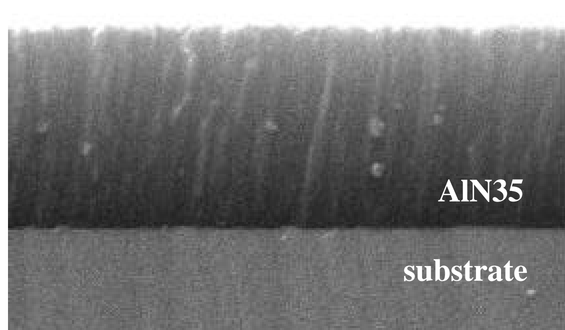

Figure 4. Cross-section SEM image of the film 1585 nm thick. The columnar structure is clearly visible.

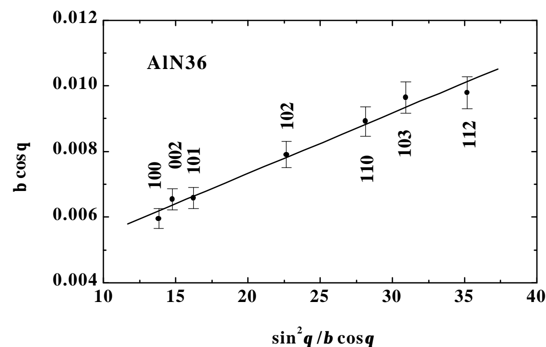

Figure 5. Williamson-Hall plot for the film 200 nm thick constructed from the set of the indicated diffractions. The grain size and rms value of microstrain are calculated from the intercept of the vertical axis and slope, respectively.

profilometry is not as accurate as ellipsometry for very thin films.

Finally, the hardness measurements were performed. The stylus was impressed into the surface with an increasing load and after reaching a pre-determined maximum value, the load was reduced and the penetration depth decreased due to the elastic recovery of the deformed material. The depth and load were continuously monitored to allow the hardness data to be derived. The hardness values were taken for the indenter impressions of 10% of the total film thickness which is usually considered as a reliable measurement, not affected by the substrate [14]. For this reason, reliable hardness values could be obtained only for the two thickest films (Table 6).

4. Discussion

The most distinct structural change with increasing film thickness is a gradual built-up of the columnar hexagonal (002) texture (Table 2). In thinner films, the column density is low and a less ordered matrix outside the columns gives a visible contribution to the 002 rocking curve (Fig. 3) while in thicker films, the columnar structure with well aligned grains occupies most of the film volume (Fig. 4). On the other hand, the texture perfection is not directly proportional to the film thickness. Particularly, the 101 diffraction is absent only in GI and BB diffraction patterns for the 800 nm thickness which results in an "infinite" texture parameter (Table 2). We verified this result by a repeated deposition of this particular thickness under the same conditions and obtained similar diffraction patterns with the only 002 and 004 diffractions in BB mode and with the dominant 002 and well resolved 103 diffractions in GI mode (Fig. 7). The presence of the latter diffraction is due to the fact that the (001) lattice planes make the smallest angle with the (103) ones, namely 31.63° in the hexagonal lattice of bulk AlN.

The structure of a thin film is the result of the processes taking place at the growing film surface. These processes are governed by an interplay between the surface migration of adatoms and the interfacial reaction in which they are involved. The built-up of the surface roughness with increasing film thickness indicates the roughening during the growth (Table 5) which occurs when the adatom mobility is limited. Obviously, the gas pressure in the reaction chamber was above the thermalization threshold, i.e. the adatoms impinged on the growing surface thermalized rather than ballistically. Such conditions are favourable for crystalline grain formation and growth. At the thickness larger than ≈800 nm, the grains presumably precluded each other in further growth and smaller grains proved to be energetically more favourable, deteriorating also the (002) texture. With a larger source-target distance and/or sputtering pressure, i.e. with more thermalized (less energetic) adatoms, we could have arrived even at a transition from the hexagonal (002) to (100) texture (c axis parallel to the substrate) as it was shown for dc sputtered AlN films previously [12].

The values of the refractive index (their average error is only 1.8 %) are not very different (Table 1) which means that the mass density of the films is not much affected by the texture perfection. On the other hand, the refractive index of AlN monocrystals amounts to 2.2 which indicates that the columnar structure in the films is rather porous and less compact. In fact, the ellipsometry is sensitive to the total electron density and does not distinguish between

Table 5. Surface roughness s determined by the atomic force microscopy and X-ray reflectivity.

Sample	AlN31	AlN33	AlN27	AlN36	AlN34	AlN16	AlN35
s_{AFM} (nm)	0.149	0.159	0.601	1.01	1.22	2.16	2.25
s_{XRR} (nm)	0.15	0.10	0.60	---	---	---	---

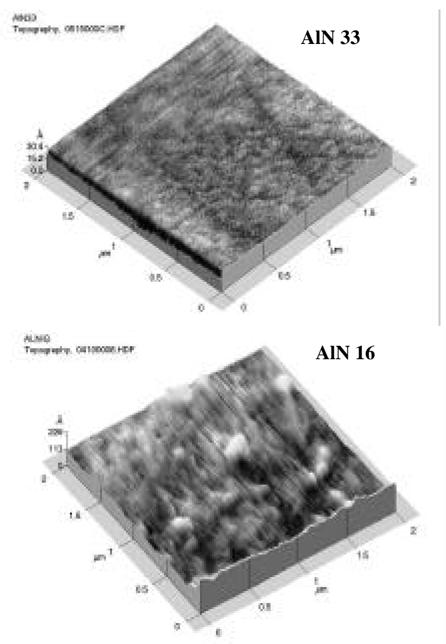

Figure 6. AFM images of the films 46 nm and 800 nm thick showing different surface morphologies.

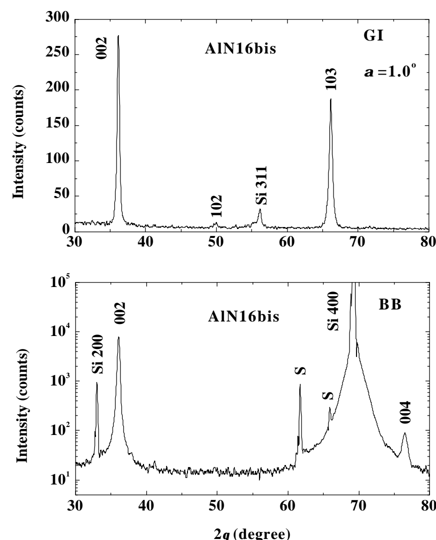

Figure 7. Grazing incidence and Bragg-Brentano diffraction patterns of the repeatedly deposited 800 nm thick film.

microscopic voids (grain boundary areas, intercolumnar space etc.) and the atomic scale voids such as vacancies.

The hexagonal wurtzite form is known as the hardest crystalline phase reported for AlN [15]. Comparing Tables 2 and 6 it can be seen that the hardness is crucially affected by the texture perfection. Presumably, better aligned grains form more distinct columns with well resolved boundaries which hamper the dislocation formation and/or motion inside the layers. .Since the hardness is dependent on the elastic properties of a material, too, different grain size and microstrain values in the films 800 nm and 1585 nm thick may also play some role. In fact, the hardness at the 800 nm thickness approaches the values reached in dc sputtered AlN films with a bias optimized for maximum hardness [5].

5. Conclusions

Highly stoichiometric AlN films in a broad thickness range from ≈10 nm to >1 μm were deposited by dc magnetron sputtering under the same conditions. The structure of AlN films is hexagonal and exhibits a transition from a fine granular to ordered columnar form with increasing film thickness. Below ≈50 nm thickness, the crystalline grains are rather small and possess the largest lattice distortion (macrostrain) and structural disorder at the atomic level (microstrain). The lattice distortion indicates a tensile in-plane stress and is relieved with increasing film thickness while the grain size and microstrain values are not affected systematically. The most important behaviour is a gradual built-up of the hexagonal (002) texture inside the columns with increasing film thickness which peaks at 800 nm. This result shows the existence of an optimized film thickness in terms of texture whose value depends on the particular deposition conditions used. Such an optimized texture apparently needn't provide a low surface roughness as the grain size grows with the texture perfection and deteriorates the surface morphology. The film thickness affects only slightly the refractive index of the films and the same is thus true for the mass density. On the other hand, the mechanical properties, particularly the hardness, are improved substantially when the texture perfection is at maximum, presumably due to the hampered dislocation formation and/or motion. The results obtained have the implications for mechanical and optical applications of AlN films.

Acknowledgements

Financial support from CONACyT of Mexico, projects No. J34225-U and G37858-E, MEC of Spain, project No. MAT99-0830-CO3-01, CE, project No. G5RD-CT-2000-00333, is acknowledged. M.J. acknowledges the support from CONACyT of Mexico within the programme Catedra Patrimonial.

References

[1] P. Vermaut, P. Ruterana, G. Nouet, Phil. Mag. **A 76**, 1215 (1997).

[2] D. Y. Wang, Y. Nagahata, M. Masuda, Y. H. Lee, J. Vac. Sci. Technol. **A 14**, 3092 (1996).

[3] Y. J. Yong, J. Y. Lee, J. Vac. Sci. Technol. **A 15**, 390 (1997).

[4] D. Liufu, .K.C. Kao, , J. Vac. Sci. Technol. **A 16**, 2360 (1998).
[5] H. Takikawa, K. Kimura, R. Miyano, T. Sakakibara, A. Bendavid, P.J. Martin, A. Matsumuro, K. Tsutsumi, Thin Sol. Films **386**, 276 (2001).
[6] T. Goto, J. Tsuneyoshi, K. Kaya, T. Hirai, J. Mat. Sci. **27**, 247 (1992).
[7] K. Jagamadham A.K. Sharma, Q. Wei, R. Kalyanraman, J. Narayan, , J. Vac. Sci. Technol. **A 18**, 2804 (1998).
[8] C. Chu, P.P. Ong, H.F. Chen, H.H. Teo, Appl. Surf. Sci. **137**, 91 (1999).
[9] M.A. Auger, R. Gago, M. Fernández, O. Sánchez, J.M. Albella, Surf. Sci. Technol. **157**, 26 (2002).
[10] M. Akiyama, C.N. Xu, T. Hagio, K. Nonaka, J. Ceram. Soc. Japan **110**, 115 (2002), 115.
[11] F. Engelmark, G.F. Iriarte, I.V. Katardijev, M. Ottosson, P. Muralt, S. Berg, J. Vac. Sci.&Techn. **A 19**, 2664 (2001).
[12] X.H. Xu, H.S. Wu, C.J. Zhang, Z.H. Jin, Thin Sol. Films **388**, 62 (2001).
[13] G.K. Williamson, W.H. Hall, Acta Metall. **1**, 22 (1953).
[14] M. Wittling, A. Bendavid, P.J. Martin, M.V. Swain, Thin Sol. Films **270**, 283 (1995).
[15] M. Ishihara, S. J. Li, H. Yumoto, K. Akashi, Y. Ide, Thin Sol. Films **316**, 152 (1998).